Melting and Degradation of Nylon-11 Particles During HVOF Combustion Spraying

Milan Ivosevic, Richard A. Cairncross, Richard Knight

Department of Chemical and Biological Engineering, Drexel University, Philadelphia, Pennsylvania 19104

ABSTRACT: Numerical predictions and experimental observations have been correlated to improve the qualitative understanding of the degree of thermal degradation occurring during the HVOF spray deposition of nylon-11. Particle residence time ($\sim$ 1 ms) in the HVOF jet was insufficient for significant decomposition of the nylon-11, but was sufficient for noticeable discoloration (yellowing) of the particles of a powder with a mean particle size of 30 μm. Experimental observation showed this to be the case even though numerical predictions indicated that the temperature of a 30 μm diameter particle should be considerably higher than the upper degradation limit of nylon-11. Initial thermal oxidation of nylon-11 promotes the formation of carbon–carbon double bonds that strongly absorb in the visible spectrum even at concentrations of parts per million causing discoloration of the nylon. © 2007 Wiley Periodicals, Inc. J Appl Polym Sci 105: 827–837, 2007

Key words: coatings; thermal spray; polymers; HVOF, degradation, modeling

INTRODUCTION

Powder coating remains one of the fastest growing industrial finishing markets, currently representing about 15% of the total, with more than 5000 operations just in North America.[1] Besides appealing finish and durability, powder coatings are also attractive to the finishing industry because of its deposition capabilities without the use of volatile organic compounds (VOCs). This is very important feature given worldwide environmental trends and the increasing number of new VOC regulations.[2] Fluidized-bed dip coating and electrostatic spray processes are considered to be two primary methods for powder coating application.[3]

An emerging technology that can also be used to deposit polymers and polymer matrix composite coatings directly from dry powders, while avoiding use of volatile organic solvents, is thermal spraying. During thermal spray deposition, high temperature, high velocity gas jets are used to accelerate and melt particulate materials injected into the jet and propel them toward the surface to be coated. Upon impact at the surface, multiple hot particles deform, cool, and consolidate to form a coating. Although thermal spraying is primarily used for the deposition of metals, ceramics, and cermets[4] to provide corrosion, wear and/or thermal protection, in recent years several authors have reported on the successful deposition of both thermosetting and thermoplastic polymers.[5–9] The key advantages of using thermal spray technology for the deposition of polymers, especially relative to electrostatic spray and fluidized-bed methods, include the ability to coat large articles in the field and to produce ''ready-to-use'' coatings without the need for postdeposition curing. Another important advantage is the ability to apply polymer matrix composite coatings with high particle reinforcement loadings (>5 vol %).[7–9] The main disadvantages include more complex processes and jet/flame temperatures of >1500°C, which can potentially degrade polymeric feedstock or previously deposited material.

One of the key questions concerning the thermal spraying of polymers is the extent of melting/degradation of polymer particles (20–200 μm) exposed to such extreme temperatures (>1500°C) for short residence times ($\sim$ 1 ms), during the particle transport through the jet. This question is addressed here for the case of thermally sprayed nylon-11 polyamide using the high velocity oxy-fuel (HVOF) combustion spray process. Numerical predictions of particle heating in an HVOF jet and experimental observations have been correlated to improve the qualitative understanding of the thermal degradation processes occurring during the HVOF spraying of nylon-11.

Background

Thermal spray is the generic term for a family of processes which use combustion flames, electric arcs, or plasma jets to melt and accelerate injected
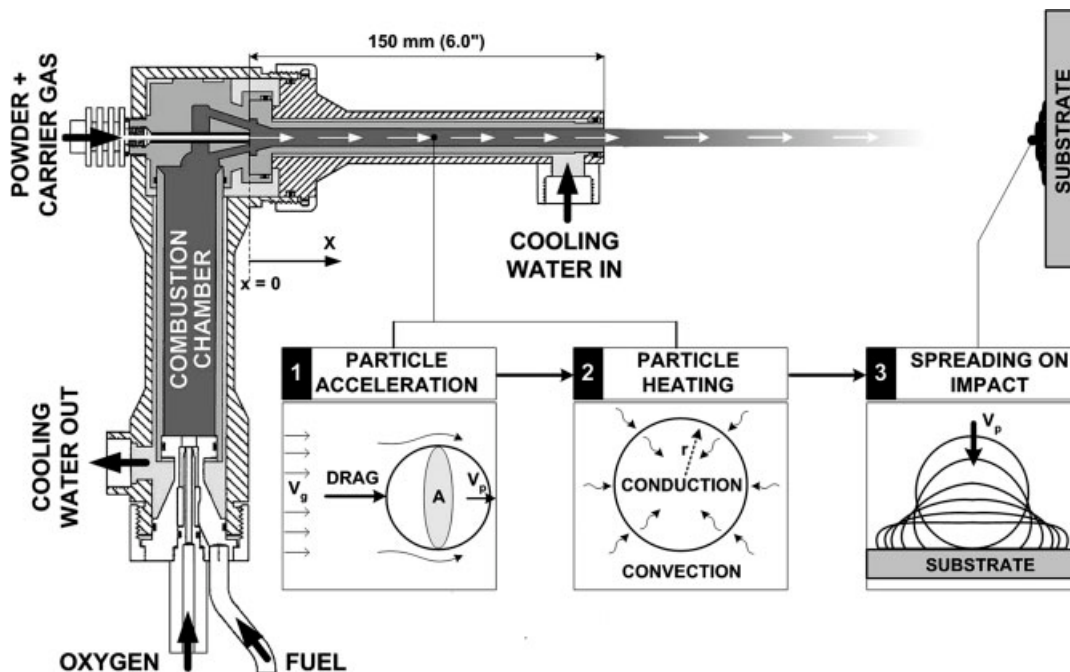
Figure 1 Schematic of the Stellite Coatings, Jet-Kote II® high velocity oxy-fuel (HVOF) thermal spray gun and three main steps in individual powder particle transport.

materials.[10] The HVOF thermal spray process, traditionally used for spraying wear-resistant cermets such as WC-Co,[10,11] was selected for spraying polymers owing to the significantly higher gas speeds (>1000 m/s) relative to other combustion-driven thermal spray processes. The ability to accelerate particles to higher speeds is important for the deposition of materials with high melt viscosity (>10^2 Pa s) such as high molecular weight polymers. A Stellite Coatings, Inc., Jet-Kote II® HVOF spray gun was used in this work. The schematic shown in Figure 1 illustrates the basic HVOF features, including an internal combustion chamber, water cooling system, particle injection into a barrel with the high-pressure combustion gases, and a rapid supersonic expansion of the combusting gases. An HVOF sprayed polymer particle is exposed to thermal environment of the jet: (i) during transport through the jet (Fig. 1, step 2) and (ii) after deposition during subsequent passes of the jet across the coating. Under certain spray conditions either or both of these exposures can potentially degrade the polymer. In addition to the jet temperature and velocity, the spray distance and torch traverse speed have been reported to have a major influence on the quality (degree of degradation) of combustion sprayed polymeric coatings[12] because the high temperature tail-flame, in conjunction with slow gun traverse speed, may cause polymer coating overheating (degradation). Moreover, the low thermal conductivity of polymers (<0.5 W/m K) results in a substantial heat accumulation at the surface of the coating so that

large temperature gradients can be developed through the coating thickness.[13,14]

The overall process control during HVOF spraying of polymers, in essence, is just a time-at-temperature particle exposure interplay such that polymer particles, exposed to combustion jet temperatures of over 1500°C, melt but do not degrade. This is possible only if the particle residence time at such high temperatures is very short. On the other hand, short residence times may not be sufficient for uniform melting of the particles. A better understanding of the melting and degradation kinetics at different temperatures would be possible if a time-temperature-transformation (degradation) diagram (TTT diagram) were available for a given material, similar in concept to those used in the curing of some thermosets.[15] The challenge for the use of TTT diagrams for thermal spraying of polymers is that the heating rates and temperature ranges in combustion jets are often significantly higher than those used to create TTT diagrams by DSC and TGA thermal analyses.

The Biot number (Bi) can also be used to obtain a better understanding of polymer particle heating characteristics inside an HVOF jet. The Biot number scales the ratio of internal and external heat transfer resistances—a high Biot number implies that internal conduction resistance dominates (i.e., polymers). The Biot number for polymers (Bi > 5) under typical spray conditions is much higher than for metals (Bi < 0.1), which implies that steep temperature gradients will develop between the core and the surface

of polymer particles. When the particle diameter is sufficiently large (>100 μm), the surface temperature can exceed the polymer degradation temperature while the core temperature stays almost unchanged. Yet, it is important to notice that the residence time at such high temperatures is very short (<1 ms) and the thickness of the exposed surface layer is also very small (∼ 1–5 μm).[16]

Nylon-11 (polyamide-11) was selected as the feedstock for the thermal spray experiments reported here, based on its industrial significance and potential in the powder coating industry. This is also one of the very few synthetic polymers to have a natural source, the nylon-11 building block is 11-aminoundecanoic acid monomer, typically synthesized from castor oil.[17] The narrow and low melting temperature region (182–191°C) makes it convenient for coating processing by electrostatic spray, fluidized-bed, and thermal spray processes. Moreover, nylon-11 has been shown to provide good resistance to corrosion, impact, abrasion, cavitation, and various chemicals.[17,18] These features make nylon-11 well suited for use as a protective coating in many industries such as water (e.g., valves, pipes, and fittings), appliances (e.g., dishwasher racks and shopping carts), petrochemical (e.g., pipes), and automotive (e.g., door rails and spline columns).[19] The nylon-11 powder used here contained no additives or pigments.

Objective

The primary objective of the research presented was to determine the extent of nylon-11 melting and degradation during HVOF thermal spray deposition using both mathematical modeling and experimental observations. A secondary objective was to define a criterion for effective deposition (i.e., without degradation) of nylon-11 polyamide using the HVOF process.

Mathematical Modeling

Detailed mathematical models used to predict particle transport and deformation on impact with a substrate during HVOF spraying of nylon-11 have been previously reported.[16] In this section, only the key aspects of this model, including the momentum and heat transfer equations for polymer particle transport in the HVOF jet are presented. The transport of a particle in an HVOF jet can be split into two separate, but dependent, parts as shown in Figure 1: (i) particle acceleration and (ii) particle heating. Particle acceleration and heating were fully coupled and simultaneously integrated within the same FORTRAN code based on the gas flow and thermal characteristics inside the HVOF gun. The gas characteristics were determined based on calculations published by

Dobbins et al.[20] using the same HVOF system as used here.

It is commonly accepted[21] that drag is the dominant force governing the motion of particles in an HVOF jet, so that particle motion can be described by the following ordinary differential equations:

$$m_{(p)}\frac{d^2x_{(p)}}{dt^2} = \frac{1}{2}C_D\rho_{(g)}A_{(p)}\left(V_{(g)} - V_{(p)}\right)\left|V_{(g)} - V_{(p)}\right|$$

$$\frac{dx}{dt} = V_{(p)}, \qquad x(0) = 0, \qquad V_{(p)}(0) = 0 \tag{1}$$

where $V_{(p)}$ is the particle axial velocity, $V_{(g)}$ is the local gas velocity, $\rho_{(g)}$ is the gas density, x is the axial distance along the gun barrel, $A_{(p)}$ is the particle projection area, and C_D is the drag coefficient. The drag coefficient (C_D) is a function of the Reynolds number of the gas as described earlier.[16]

The equations describing the heat transfer from the gas to a single spherical particle (assuming spherical symmetry) with appropriate initial and boundary conditions will be as follows:

$$\rho_{(p)}C_{P(p)}\frac{\partial T_{(p)}}{\partial t} = \frac{1}{r^2}\frac{\partial}{\partial r}\left(r^2k_{(p)}\frac{\partial T_{(p)}}{\partial r}\right),$$

$$T_{(p)}(r, t = 0) = T^0_{(p)}$$

$$\frac{dT_{(p)}}{dr}\left(r = 0, t\right) = 0, \qquad -k_{(p)}\frac{dT_{(p)}}{dr}\left(r = R_{(p)}\right)$$
$$= h\left(T_{(p)}(R_p) - T_g\right) \tag{2}$$

where $T_{(p)}$ is the particle temperature, and $\rho_{(p)}$, $Cp_{(p)}$, and $k_{(p)}$ are the density, heat capacity, and thermal conductivity of the particle, r is the radial distance from the center of the particle, $(R = D/2)$ is the particle radius and h is the heat transfer coefficient. The heat transfer coefficient, (h), was computed using the Ranz–Marshall semiempirical equation.[22] Within the mathematical model of heat transfer [eq. (2)], the heat consumed by melting of the polymer was accounted for by making the polymer heat capacity $Cp_{(p)}$ a function of temperature using the apparent heat capacity method, as described by Hu and Argyropoulos.[23] For all simulations, except where stated otherwise, the parameters listed in Table I were used.

TABLE I
Parameters used in Mathematical Modeling

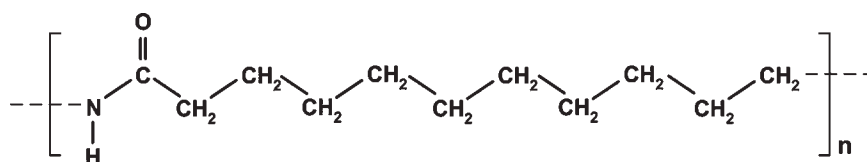| Nylon-11 particle	HVOF gas (superheated steam at 2000 K)
$\rho_{(p)} = 1030$ g/cm^3	$\rho_{(g)} = 0.15$ g/cm^3
$k_{(p)} = 0.19$ W/m K	$k_{(g)} = 0.20$ W/m K
$\Delta H_f = 72.2$ J/g	$\mu_{(g)} = 7 \times 10^{-5}$ Pas s
$Cp_{(p)} = 1753$ J/kg K	$Cp_{(g)} = 5000$ J/kg K

Figure 2 Molecular structure of nylon-11 (poly(11-aminoundecanoic acid)).

Equations (1)–(2) for momentum and heat transfer were solved by numerical integration using the forward Euler method with a time step small enough (10^{-7} s) that the local Reynolds number, gas velocity and temperature could be considered constant over each time step.[16]

EXPERIMENTAL

Material

Semicrystalline nylon-11 (polyamide-11) powder, commercially available as Rilsan® D: PA-11 French Natural ES (donated by Arkema, Inc., King of Prussia, PA) was used as the feedstock for the thermal spray experiments reported. The molecular structure of this thermoplastic polymer is shown in Figure 2. The melting and degradation temperatures of nylon-11, as reported by the manufacturer and confirmed in this study, were in the range ∼ 180–190°C and 350–550°C, respectively. Three different powder size distributions [Fig. 3(a)] with mean particle sizes of 30 μm (D-30), 60 μm (D-60), and 120 μm (D-120), and angular powder morphology [Fig. 3(b)] were evaluated and compared in the experiments reported.

Thermal spray experiments

All three nylon-11 powders: D-30, D-60, and D-120, [Fig. 3(a)], were thermally sprayed using the same HVOF spray conditions. The experiments were carried out using a Stellite Coatings, Inc. (Goshen, IN), Jet-Kote II® HVOF spray system (Fig. 1) with oxygen and hydrogen flow rates of 0.0024/0.0039 m^3/s (300/500 scfh), respectively, and a spray distance of 225 mm. The spray nozzle used was 150 mm long with an internal diameter of 6.4 mm.

First, swipe or ''splat'' tests comprising single high speed (>0.7 m/s) passes of the spray gun across room temperature glass slides, were conducted at low powder feed rates (∼ 2 g/min) to observe the morphology of individual splats. Then, the same powder feed rate, equipment, and other spray parameters were used to deposit ∼ 500–600 μm thick nylon-11 coatings on grit blasted 1018 steel substrates. The materials were deposited using high traverse gun speed (>0.7 m/s), followed by external compressed air (410 kPas or 60 psi) cooling for 30 s from the distance of 100 mm, to minimize the effect of postdeposition heating during the subsequent jet passes

across the coating. This technique helped to deposit individual spats and coatings which mainly reflect features generated by thermal history of the particles during heating inside the spray gun. Post-deposition, melting/fusing of combustion spray polymer particles is beyond the scope of this paper.
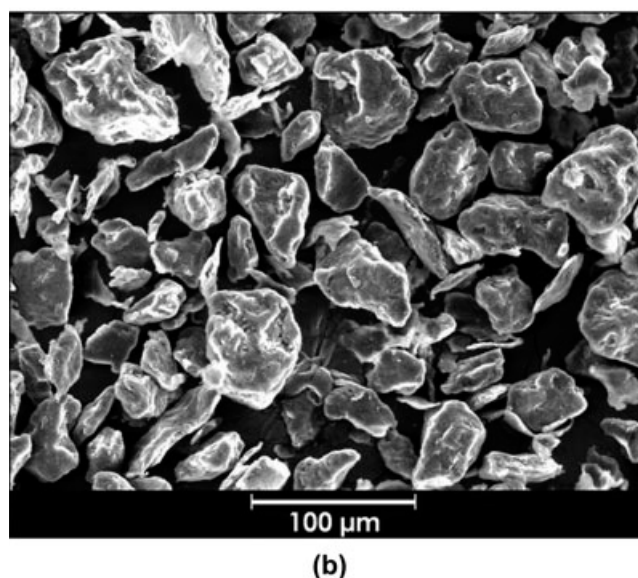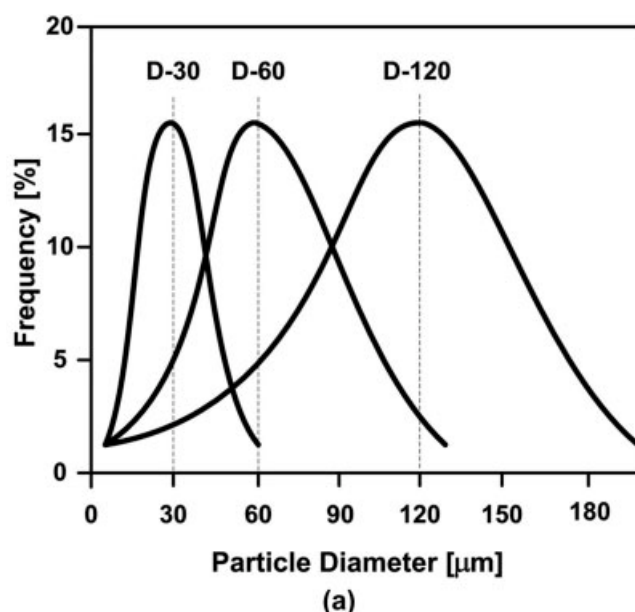

(a)

(b)

Figure 3 Nylom-11 powder. (a) Particle size distributions as reported by the manufacturer for D-30, D-60, and D-120 powders. (b) SEM image showing typical D-60 powder morphology.

One of the important characteristics of thermal spraying in general is that a relatively large number of process parameters need to be controlled during the spray process. Although this is often challenging with respect to process repeatability, it also increases the number of parameter combinations that can be varied to achieve specific coating microstructures. Normally spray parameters would be optimized for each powder size, however, in this work the selected spray parameters were chosen as a baseline and held constant to observe the effect of variations in powder size.

Coating characterization

Cross-sectional samples of sprayed coatings were prepared using standard metallographic techniques: sectioning, mounting, and polishing. The coating cross section and splat morphologies were analyzed by optical microscopy using an Olympus PMG-3 optical metallograph.

Thermal properties of the coatings and the powders, including heat of fusion, glass transition, melting, and degradation temperatures, were characterized by differential scanning calorimetry (DSC) and thermogravimetric analysis (TGA) (Perkin–Elmer, Waltham, MA models DSC-7 and TGA-7). DSC was carried out at heating and cooling rates of $10°C$ min^{-1} in nitrogen to produce second heating scans and eliminate potential thermal history effects of the materials. TGA scans were carried out in air over a temperature range of $25-600°C$ with a heating rate of $20°C$ min^{-1}.

Fourier transform infrared spectroscopy (FTIR) was used to characterize polymer degradation by tracking changes in molecular bonding. FTIR spectra of the coatings and as-received powders were obtained using an Excalibur FTS-3000 spectrometer (Varian, Inc., Palo Alto, CA) with an accompanying UMA 600 microscope.

RESULTS AND DISCUSSION

Predicted particle velocity and temperature

The acceleration of particles in the HVOF jet was predicted by solving eq. (1), and the results are shown in Figure 4. The predicted velocities of 30, 60, and 120 μm diameter particles at the moment of impact on the substrate at a spray distance of 225 mm and given spray conditions were 537, 497, and 368 m/s. The residence times of 30, 60, and 120 μm diameter particles inside the HVOF jet were 0.7, 1.0, and 1.4 ms [Fig. 4(b)]. The residence or the time of particle exposure to the forced convection of the HVOF jet is critical for the heat transfer calculations.

The heat transfer from the combusting gas to the nylon-11 particles was predicted by solving eq. (2). The temperature of a single 120 μm particle
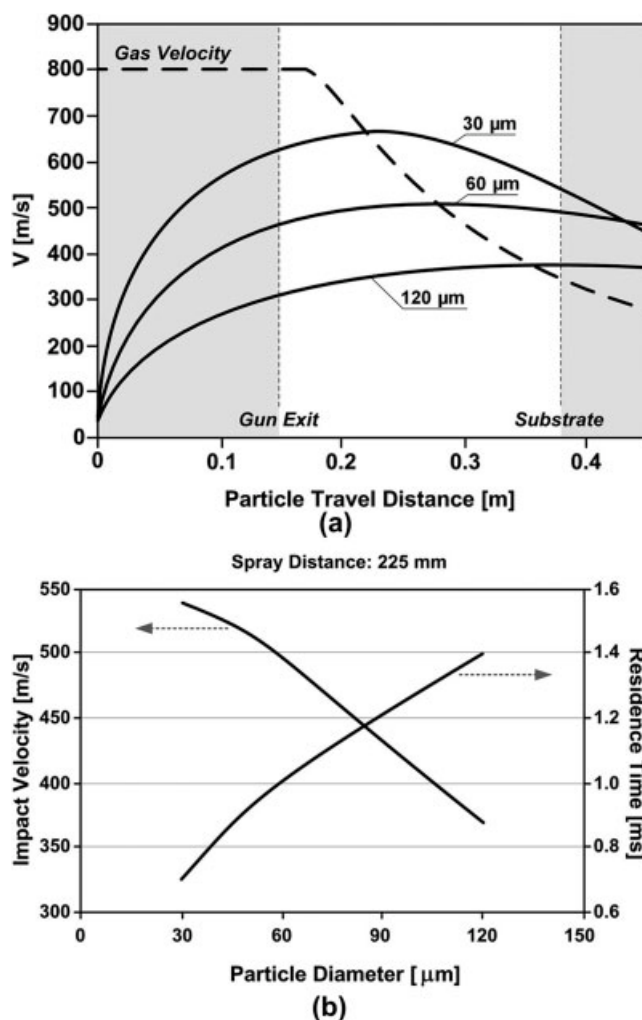

Figure 4 Predicted particle velocities. (a) Particle and gas velocities as a function of travel distance. (b) Particle impact velocities and residence times as a function of particle size.

with respect to travel distance is shown in Figure 5(a), and the predicted temperature profiles within 30, 60, and 120 μm diameter particles immediately before impact with a substrate are shown in Figure 5(b).

Forced convection from the HVOF jet to micronscale particles is characterized by a large convective heat transfer coefficient ($h \sim 5000-17,000$ W/(m^2 K)), which will be higher for smaller diameter particles. Smaller particles heat up faster due to: (i) their higher surface area to volume ratio and (ii) higher convective heat flux, because the heat transfer coefficient (h) is inversely proportional to the particle diameter, as indicated by the Ranz–Marshall equation.[22] These factors ensure that a 30 μm particle develops an unrealistically high predicted particle temperature (>1200°C), well above the upper degradation limit of nylon-11 (557°C). The model predicts that a 30 μm particle even develops an inverted temperature profile, with a higher temperature in the core than at the surface
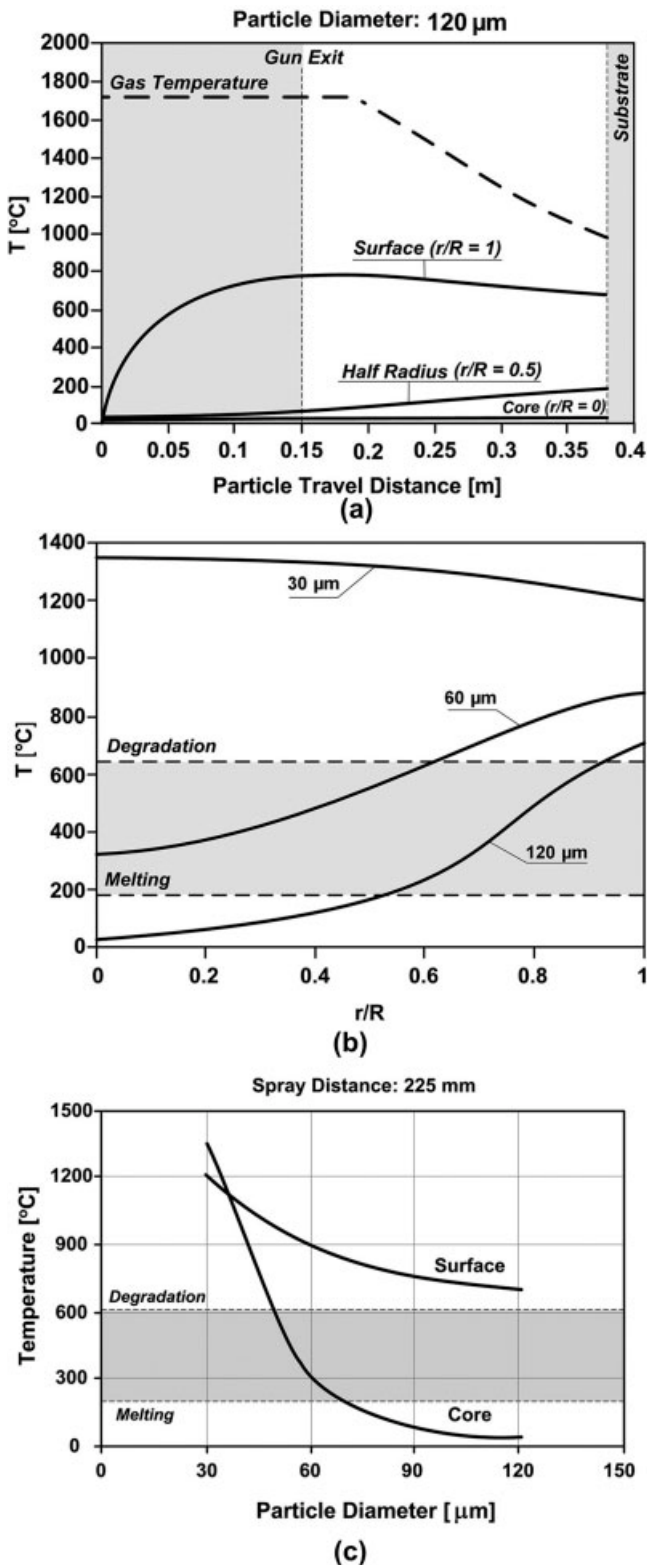
Figure 5 (a) Temperature profiles of a 120 μm diameter nylon-11 particle as a function of travel distance. (b) Temperature profiles of different particle diameters immediately before impact with a substrate at 225 mm spray distance. (c) Temperature profiles of the core and surface of particles at the moment of impact with the substrate.

[Fig. 5(b, c)]. The inversed profile is caused by gas temperature that decreases as the gas expands further from the gun exit [Fig. 5(a)] and becomes lower than the particle surface temperature.

High temperatures (>1500°C) and short residence times (~ 1.4 ms) are also responsible for a rapid increase in polymer particle surface temperature, which for a 120 μm diameter particle reaches almost ~ 700°C within the spray nozzle [Fig. 5(a)]. Despite the rapid rise in particle surface temperature, the high internal thermal resistance (high Bi number) of nylon-11 particles prevents the interior of the particle from being heated at the same rate. Furthermore, the 120 μm diameter particle was predicted to have an unmelted core and surface temperature above the degradation temperature, whereas a 60 μm diameter particle was predicted to be fully melted, but with almost 70% of its volume above the degradation temperature [Fig. 5(b, c) and Table II].
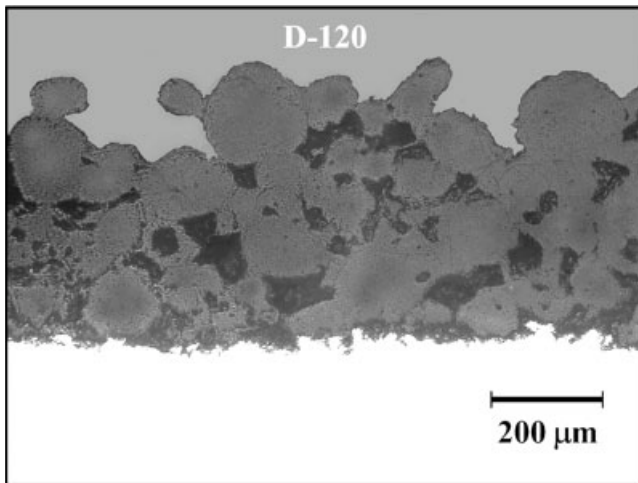
According to the numerical predictions, particles smaller than ~ 40 μm in diameter and the surfaces of larger particles should exceed the degradation temperature of nylon-11 under the spray conditions used. It is not clear whether degradation occurs during such short particle residence time (~ 0.7–1.5 ms) in the jet as the mathematical models used here do not include any polymer degradation kinetics. The issue of degradation during thermal spraying of nylon-11 is addressed in the following sections via experimental observations of coatings deposited under the same HVOF conditions using powders with mean particle size distributions of (30, 60, and 120 μm).
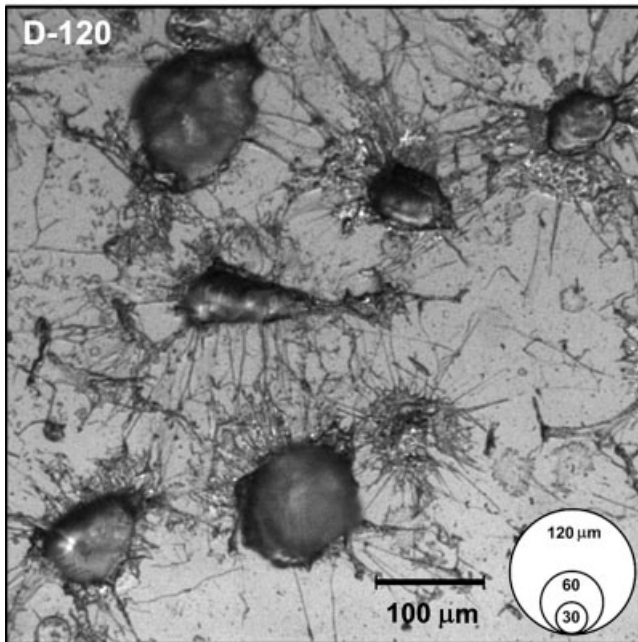
Coating microstructures

The coating microstructures and corresponding individual particle splats produced from the three nylon-11 powders used are shown in Figures 6–8. The microstructure of the D-120 coating [Fig. 6(a)] appeared to be very porous, consisting of large rounded, incompletely fused polymer particles, and an irregular rough surface. The porous microstructure likely resulted from incomplete melting of the coarse nylon-11 particles, i.e., melted surfaces and unmelted cores. This was consistent with the predicted

TABLE II
Predicted Particle Volume Fraction Above the Melting and Degradation Temperatures

| Particle diameter (μm)	Vol. (%) above melting temperature (>190°C)	Vol. (%) above upper degradation limit (>600°C)
30	100	100
60	100	74
120	86	19

Figure 6 HVOF sprayed D-120 nylon-11 powder. (a) Coating. (b) Individual splats captured on a glass slide.

temperature profile for a 120 μm diameter particle shown in Figure 5. The large, partially melted, particles also generated "chunky" and poorly deformed splats as can be observed in Figure 6(b).

The microstructure of the D-60 coating [Fig. 7(a)] had a significantly lower degree of porosity than the D-120 coating indicating a higher degree of particle melting and splatting [Fig. 7(b)]. This was also consistent with the numerical calculations where a 60 μm diameter particle was predicted to be fully melted. Interestingly, it was also predicted [Fig. 5(b)] that the temperature of a 30 μm diameter particle would be significantly higher (>1200°C) than the upper degradation limit of nylon-11 (557°C), indicating the possibility of complete decomposition (burning) of these

particles under the selected HVOF conditions. Yet, the D-30 material was successfully deposited, producing a dense and adherent coating [Fig. 8(a)] with well-deformed splats [Fig. 8(b)]. Apparently, a particle residence time of less than 1 ms at temperatures exceeding 1500°C was insufficient for complete burning of the D-30 powder during HVOF spraying.

On the other hand, the appearance of the three coatings was significantly different, as shown in Figure 9. The D-30 coating exhibited significant discoloration (yellowing) as a result of oxidation and/or other degradation processes such as main chain scission and/or crosslinking. The D-60 showed slight discoloration and the D-120 coating appeared the same as the initial powder with little or no yellowing observed
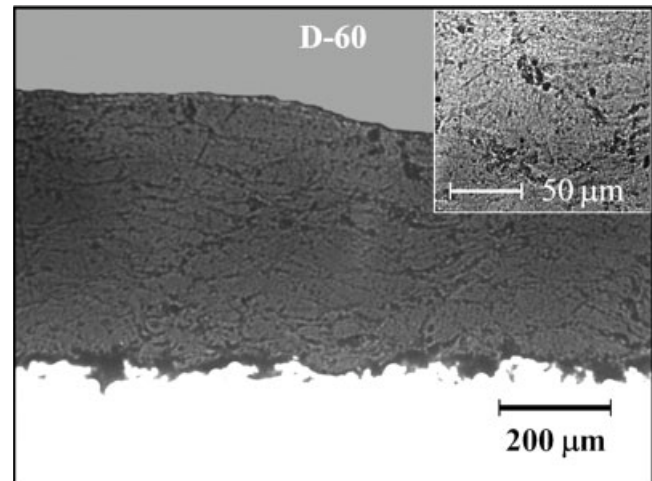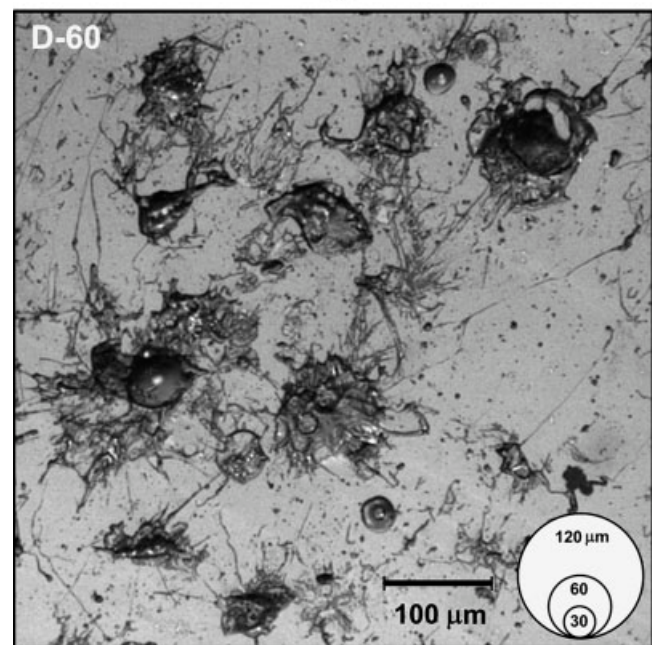
Figure 7 HVOF sprayed D-60 nylon-11 powder. (a) Coating. (b) Individual splats captured on a glass slide.
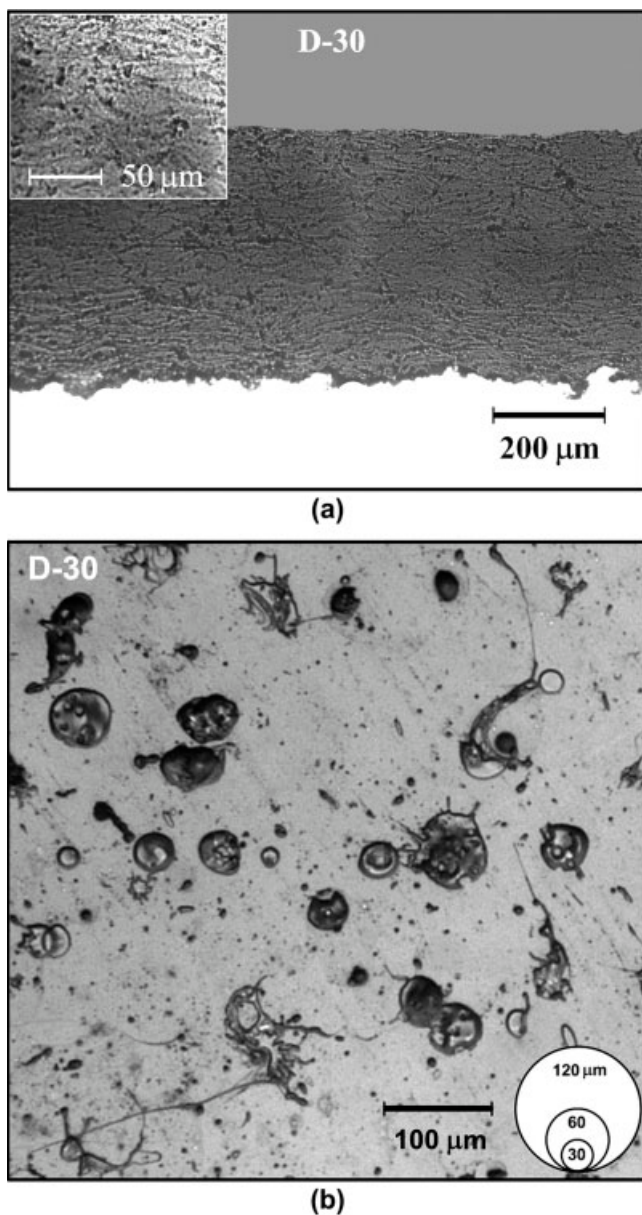
Figure 8 HVOF sprayed D-30 nylon-11 powder. (a) Coating. (b) Individual splats captured on a glass slide.

(Fig. 9). Theoretically, even slight yellowing of nylon-11 is an indicator of the onset of molecular structure change due to oxidative developments.[24]

Degradation of nylon-11 coatings

The D-30 coatings deposited using nylon-11 powder with the smallest mean particle size ($\sim$ 30 μm) exhibited the most significant color change (Fig. 9) owing to the most intense heating in the HVOF jet, as explained earlier. Therefore, this coating was used to determine the extent of thermal degradation of nylon-11 during HVOF spray process, assuming that the D-60 and D-120 coatings had lower degrees of degradation.

The thermal properties of the nylon-11 D-30 coating and as-received D-30 powder, including DSC and TGA scans, are shown in Figure 10. It was expected that changes in molecular weight, due to degradation including main chain scission and/or crosslinking, would reflect in changes in crystallinity, glass transition, melting, and/or degradation temperatures of the coatings when compared with the original powder. The glass transition temperature of nylon-11, as reported by the manufacturer, is between 40 and 50°C. In the DSC second heating scan [Fig. 10(a)], the glass transition was not sufficiently distinct to be useable for comparing the D-30 coating and powder. Moreover, a negligible difference in the heat of fusion (56 and 59 J/g) between the coating and powder was determined, indicating only minor difference in the crystallinity level. Discoloration of the D-30 coating after HVOF spraying appeared to have minor effects on the thermal properties of the nylon-11. Similarly, no major differences were found between the D-30 powder and coating in the TGA scans [Fig. 10(b)], implying that the yellowing of the nylon-11 D-30 coating also did not affect the onset of the main mass loss degradation temperature that occurred around 350°C. The D-60 and D-120 coatings and powders exhibited the same DSC/TGA characteristics as the
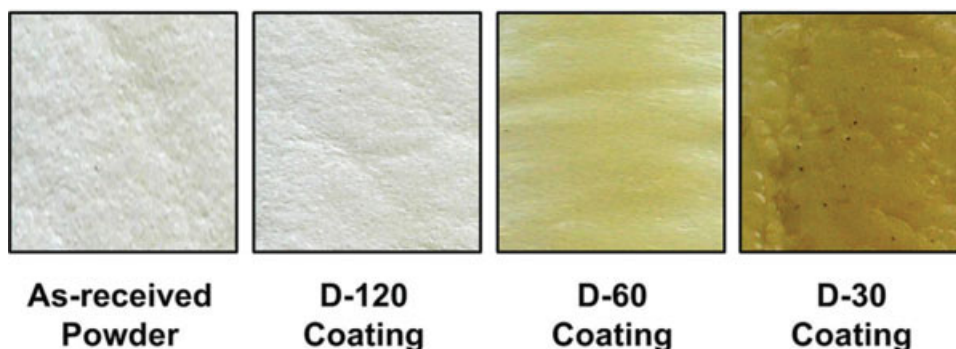

Figure 9 Appearance of D-120, D-60, and D-30 coatings relative to the as-received nylon-11 powder. [Color figure can be viewed in the online issue, which is available at www.interscience.wiley.com.]
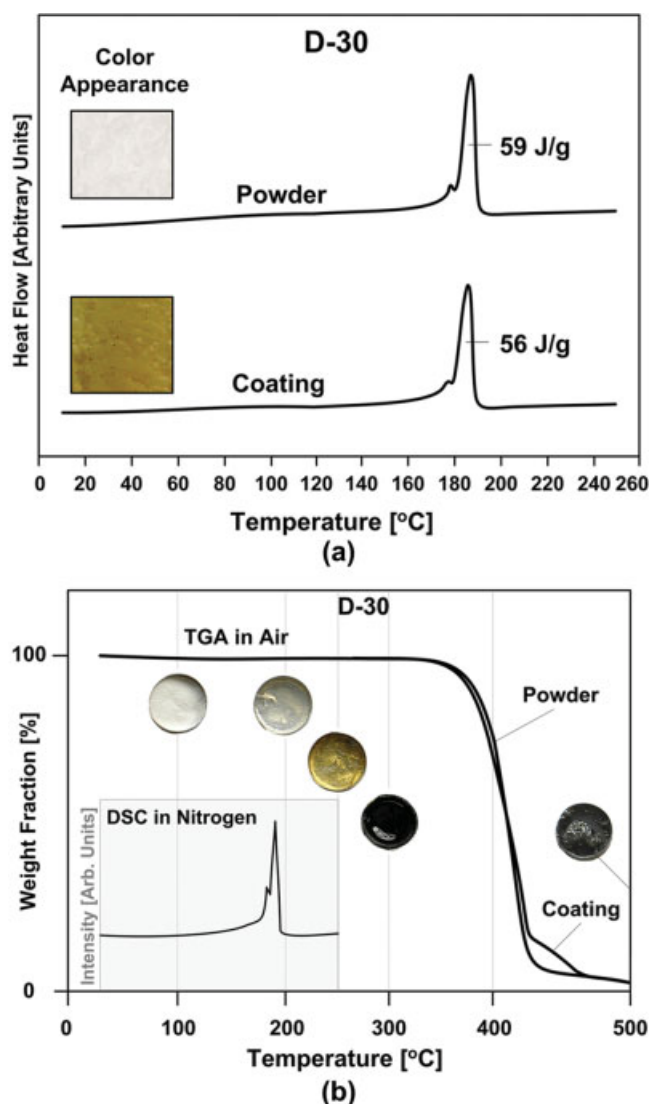
Figure 10 Thermal properties of nylon-11 D-30 coating and powder. (a) DSC thermograms. (b) TGA scans. [Color figure can be viewed in the online issue, which is available at www.interscience.wiley.com.]

D-30 coating and powder (Fig. 10). Interestingly, it was observed that discoloration of as-received nylon-11 powder could occur when the material was heated to different temperatures in air. For example, nylon-11 D-30 powder samples heated in air at 10°C/min to temperatures of 200, 250, and 300°C and then cooled at the same rate had noticeably different appearances after heating—samples heated to the higher temperature were darker in color [Fig. 10(b)]. This was not observed when powder was heated in nitrogen, indicating that the discoloration observed was likely caused by an oxidative process. The kinetics of the thermal oxidation of nylon-11 at different temperatures (i.e., time-temperature-transformation diagrams) is beyond the scope of this article.

FTIR analysis did not reveal the presence of any degradation products, nor did it indicate any

significant difference between as-received and HVOF sprayed D-30 nylon-11 (Fig. 11). Similar observations on HVOF sprayed nylon-11 coatings were previously reported by Petrovicova et al.[7] This was surprising since the D-30 coating discoloration was considerable. A possible explanation for FTIR not indicating any molecular changes in HVOF sprayed D-30 coatings can be found in the thermo-oxidative mechanisms of nylon-11 (Fig. 12).[24] Thermal oxidation is initiated by the abstraction of a hydrogen atom from a nitrogen-vicinal methylene group.[24,25] The radical formed in the initial oxidation step at the nitrogen-vicinal methylene group then combines with oxygen to form a new radical, which may isomerize or follow various reaction pathways (each involving chain scission) resulting in the formation of carbonyl groups and carboxyl end-groups. During the initial stage of thermal oxidation of nylon-11 and conjugation of carbonyl groups, $C = C$ double bonds could be formed (Fig. 12, detail A). These double bonds, even at concentrations of parts per million (ppm) can noticeably change the optical properties of the polymer, resulting in discoloration of the nylon-11.[26] Such small concentrations (i.e., <1%) of $C = C$ double bonds that affects the coating appearance may be insufficient to be detected by FTIR spectroscopy. Even the noticeable discoloration of HVOF deposited nylon-11 coatings did not reflect on the thermal properties of the material or chemical structure to a large extent; this still does not guarantee that the coating retained its original, nonoxidized, mechanical properties. It was reported[24] that aliphatic nylons exposed to prolonged heating become brittle due to crosslinking and decomposition. A simple tensile or 3-point bend test could be use to determine the extent of damage that thermal oxidation (discoloration) has on the mechanical properties of nylon-11. This topic is beyond the scope of this work and will be treated as a separate
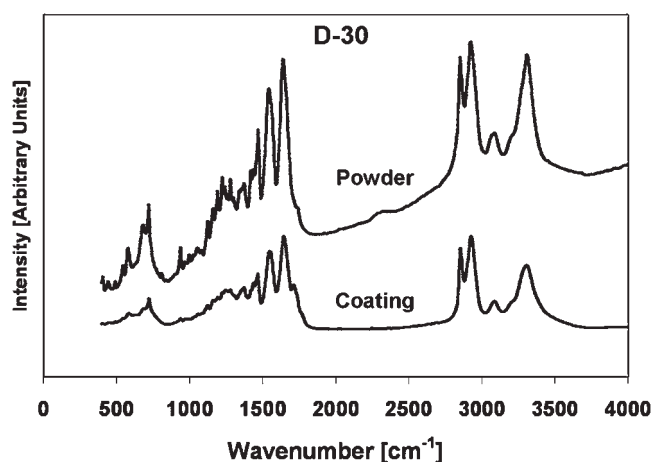

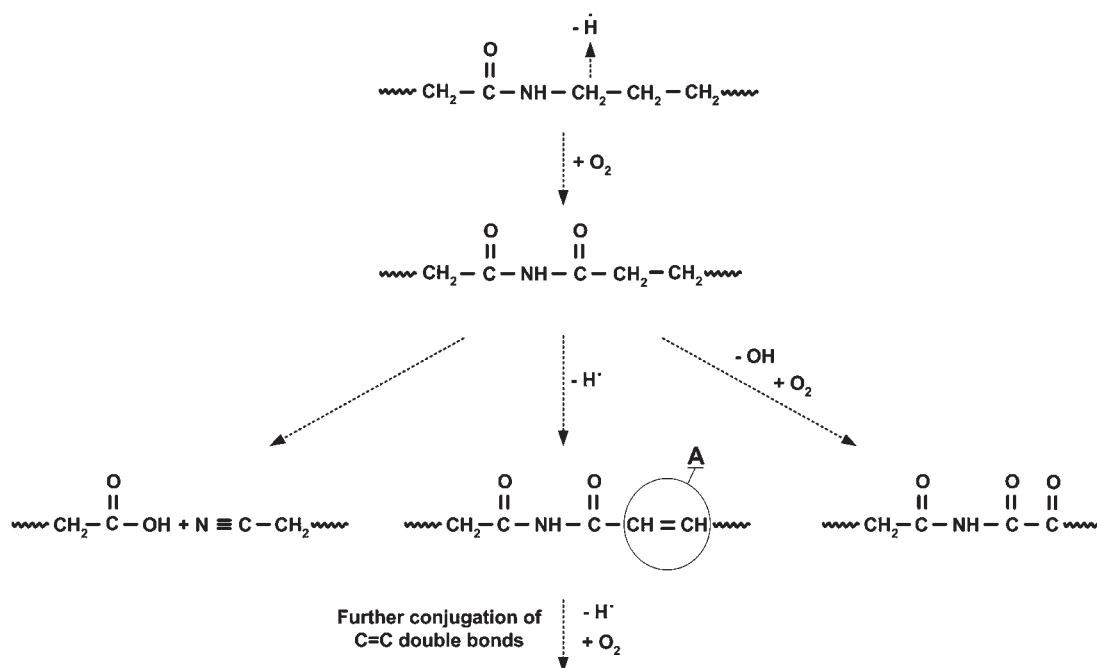**Figure 11** FTIR spectra of nylon-11 D-30 coating and as-received powder.

Figure 12   Thermo-oxidative degradation mechanism of nylon-11.[24]

subject. On the other hand, the yellowing of nylon-11, apparently, can be used as an indicator for the optimization of the HVOF spray parameters. The HVOF spray parameters, primarily fuel:oxygen ratio, spray distance, gun surface speed, and feedstock powder size distribution, should be selected such that little or no discoloration of the white nylon-11 occurs, similarly to that of D-60 and D-120 coatings shown in Figure 9.

CONCLUSIONS

One of the principal goals of this work was to develop a knowledge base and improved qualitative understanding of the potential degradation mechanisms, including thermal oxidation, during the HVOF combustion spraying of nylon-11. Numerically predicted temperatures of 30, 60, and 120 μm diameter particles were correlated to experimental observations of coatings deposited under the same HVOF conditions using powders of three different mean particle sizes [30 μm (D-30), 60 μm (D-60), and 120 μm (D-120)]. All three powders were successfully deposited, producing coatings with different levels of porosity, the most porous coating corresponding to the coarsest feedstock powder ($\sim$ 120 μm). The D-30 coating was successfully deposited, even though numerical predictions indicated that the temperature of a 30 μm diameter particle should be considerably higher than the upper degradation limit of nylon-11. Apparently, the typical particle residence time of less than 1 ms in the high temperature jet ($>1500°C$) was insufficient

for significant thermal decomposition (burning) of the D-30 powder to occur during HVOF spraying. Although the D-30 coating was dense and adherent, it exhibited considerable discoloration (yellowing) as a result of thermal oxidation during HVOF spraying. The D-60 coating showed slight discoloration, and no yellowing was observed in the D-120 coating. Nevertheless, significant discoloration of the D-30 coating did not correspond to any change of thermal properties of the coating relative to the original powder, including crystallinity, glass transition, melting, and/or degradation temperatures. FTIR analysis also did not reveal the presence of any degradation products, nor did it reflect any significant difference between the as-received powder and sprayed D-30 nylon-11. It was assumed that during the initial stage of thermal oxidation of nylon-11, $C = C$ double bonds were formed. These double bonds, even in concentration of the order of parts per million (ppm) strongly absorb in the visible spectrum, resulting in discoloration of the nylon-11, but remain undetectable by FTIR spectroscopy. It was concluded that yellowing of the nylon-11, apparently, can be used as an indicator for the optimization of the HVOF process parameters, which should be chosen such that little or no discoloration of the white nylon-11 occurs to preserve the properties of this material.

References

1. Zimoch, R. Mod Metals 2003, 59, 36.
2. Randall, P.M. J Hazard Mater 1992, 29, 275.
3. Cowley, M. Finishing 2002, 26, 32.
4. Fauchais, P.; Vardelle, A.; Dussoubs, B. J Therm Spray Technol 2005, 10, 44.
5. Zhang, T.; Gawne, D. T.; Bao, Y. Surf Coat Technol 1997, 96, 337.
6. Brogan, J. A.; Berndt, C. C. J Mater Sci 1997, 32, 2099.
7. Petrovicova, E.; Knight, R.; Schadler, L. S.; Twardowski, T. E. J Appl Polym Sci 2000, 77, 1684.
8. Petrovicova, E.; Schadler, L. S. Int Mater Rev 2002, 47, 169.
9. Ivosevic, M.; Knight, R.; Kalidindi, S. R.; Palmese G. R.; Sutter, J. K. J Therm Spray Technol 2005, 14, 45.
10. Davis, J. R., Eds.; Handbook of Thermal Spray Technology, 1st ed.; ASM International: Materials Park, OH, 2004.
11. Thorpe, M. L.; Richter, H. J. J Therm Spray Technol 1992, 1, 161.
12. Zhang, T.; Gawne, D. T.; Bao, Y. In Proceedings of the 9th National Thermal Spray Conference. Thermal Spray: Practical Solutions for Engineering Problems; Berndt, C. C., Ed.; ASM International: Materials Park, OH, 1996, p 231.
13. Gawne, D. T.; Zhang, T.; Bao, Y. In Proceedings of the ITSC-2001, Singapore; ASM International: Materials Park, OH, 2001, p 307.
14. Ivosevic, M.; Knight, R.; Kalidindi, S. R.; Palmese, G. R.; Sutter, J. K.; Tsurikov, A. In Proceedings of the ITSC-2003, Orlando, FL; Moreau, C., Ed.; ASM International: Materials Park, OH, 2003.
15. Chan, L. C.; Naé, N. N.; Gillham, J. K. J Appl Polym Sci 1984, 29, 3307.
16. Ivosevic, M.; Cairncross, R. A.; Knight, R. Int J Heat Mass Transfer 2006, 49, 3285.
17. Apgar, G. B. In PA-11, Nylon Plastic Handbook; Kohan, M., Ed.; Hanser/Gardner Publications: Cincinnati, OH, 1995.
18. McAndrew, T. P.; Audenaert, M.; Petersheim, J.; Garcia, D.; Richards, T. Polym Prepr (Am Chem Soc Div Polym Chem) 2004, 45, 155.
19. McAndrew, T. P.; Cere, F. Presented at the 2006 International Thermal Spray Conference (ITSC-2006), DVS/IIW/ASM-TSS; Seattle, WA, ASM International, Materials Park, OH, May 15–18, 2006.
20. Dobbins, T. A.; Knight, R.; Mayo, M. J. J Therm Spray Technol 2003, 12, 214.
21. Cheng, D.; Trapaga, G.; McKelling, J. W.; Lavernia, E. J. Key Eng Mater 2001, 197, 1.
22. Bird, R. B.; Stewart, W. E.; Lightfoot, E. N. Transport Phenomena; Wiley: New York, 1960.
23. Hu, H.; Argyropoulos, S. A. Modell Simul Mater Sci Eng 1996, 4, 371.
24. Levchik, S. V.; Weil, E. D.; Lewin, M. Polym Int 1999, 48, 532.
25. Lehrle, R. S.; Parsons, I. W.; Rollinson, M. Polym Degrad Stab 2000, 67, 21.
26. Li, R.; Hu, X. Polym Degrad Stab 1998, 62, 523.